An Investigation of Boundary Layer Depth Retrieval and Characteristics from the SPARC Trailer at the Park Falls WLEF Tall Tower

Author: Kip Nielsen

Advisor: Ankur Desai

Abstract

A correlation and interrelationship across a wide variety of instruments provided by the University of Wisconsin – Madison's Space Science and Engineering Center's Portable Atmospheric Research Center (SPARC) gives insight for observing boundary layer characteristics. The SPARC was positioned near the WLEF tall tower in Chequamegon-Nicolet National Forest in northern Wisconsin for September 23rd and 24th, 2016. The SPARC's high resolution spectral lidar showed clear evidence of a mixed layer starting near 13:00UTC on September 23rd. The SPARC also provides an atmospheric emitted radiance interferometer whose accuracy is unconfirmed due to significant departures from the September 24th radiosonde launched at 19:14UTC. There was also a WindPro lidar in the suite but was highly imprecise arising from a low signal-to-noise ratio. The WLEF tower showed carbon dioxide to be more uniform when a mixed layer was evident (13:00UTC-24:00UTC on September 23rd). Sensible heat and latent heat fluxes from the tower were directly correlated with the interferometer's temperature profiles. The friction velocity measured from the tower was consistently related to the amount of convection seen from the spectral lidar. The SPARC's surface meteorology station showed a reduction in 1.5 hPa of pressure on September 24th at 19:00UTC providing some evidence for a low-pressure front. A separate analysis when the WLEF has accurate soil moisture, sensible heat, latent heat, and friction velocity measurements would provide more insight. Additionally, the WindPro lidar would need to be observed when the data provides a signal-to-noise ratio that is at least greater than .008 to properly deduce boundary layer characteristics.

Introduction

The boundary layer (BL) is an expansive characteristic of earth and is crucial to understand for properly analyzing atmospheric phenomena. The BL can also go by planetary boundary layer or atmospheric boundary layer, but it essentially measures the interaction between the surface and the atmosphere. Its depth and thickness generally varies between 1.0-2.0km but may even go above 4.0km in the troposphere arising from mechanical and thermal turbulence. Mechanical turbulence is caused by the interaction between vegetation and wind patterns. Thermal turbulence occurs due to solar radiance emitted from the sun and generally produces much stronger convection than its wind-driven counterpart. However, both mechanical and thermal turbulence combine with equal intensity to form the shallow surface layer during the day as shown in Figure 1.

The convection from thermal turbulence is initiated via surface heating from the surface becoming warmer than the air above it, creating an inversion. These air parcels will be warmer and therefore have higher buoyancy and can create lift, otherwise known as convection. Since the BL is strongly influenced by the surface energy balance between shortwave solar energy and longwave thermal emittance, greenhouse constituents and cloud thickness become important. More specifically, carbon dioxide has an absorption band with peaks near 2.8μm and 4.3μm showing its importance when considering the longwave emittance from earth. The BL formed during the day is known as the convective boundary layer or mixed layer and is caused by convection that starts in the morning from increased incoming solar radiation. This layer is associated with potential temperature showing a small inversion near the surface, uniformity along the layer and stratification further aloft. Dust particle concentration is generally high and uniform throughout this layer showing that pollution is generally well-mixed. On the other hand, a nocturnal boundary layer, or stable boundary layer, is formed at night mainly due to wind

speed and surface friction, and is generally much thinner than the mixed layer. Above this stable layer is the residual layer which is an inactive, well-mixed layer that forms right after sunset. It generally consists of uniformity based on characteristics from the daytime mixed layer and is only altered via horizontal advection or radiative cooling.

Regardless of the time of day, the BL always has either a capping inversion or entrainment zone above the residual or mixed layer, respectively. This is due to the instability within the BL being significantly different from the free atmosphere above, making the overall layer become more pronounced. The capping inversion forms during the night and is a strong stable layer that connects to the free atmosphere above it and essentially traps the turbulence in the BL. The stronger the capping inversion from a change in potential temperature, the less the overall entrainment. There is generally a sharp gradient in humidity across the capping inversion arising from the mixed layer having a higher Water Vapor Mixing Ratio (WVMR) than the free atmosphere above as caused by daytime evaporation. The entrainment zone is the same as the capping inversion but only occurs between sunrise and sunset. A previous comparison of BL depth across different instruments showed that it was more reliable to analyze the diurnal cycles between the instruments instead of attempting to observe the transition between the capping inversion or the entrainment zone and the free atmosphere (Sawyer and Li, 2013). This is consistent with motivation for this analysis due to all the instruments except the radiosonde being ground based and recording stronger observations at lower altitudes.

To properly analyze the BL and its daily evolution, it's crucial to look at it from a variety of perspectives. Prior studies have shown that the BL shows a positive feedback between soil moisture and rainfall on a diurnal cycle (Betts and Ball, 1998). During warmer soil temperatures, the diurnal cycle can be split in two by composting the surface flux and thermodynamic data as a

function of soil moisture to ultimately determine the effects of soil moisture (Betts and Ball, 1995). However, BL depth and progression as well as surface fluxes is caused by the atmospheric thermodynamic structure and transpiration more than variability in soil moisture, especially across a variety of spatial scales (Desai et al., 2006). Typical atmospheric thermodynamic structures of wind speed, potential temperature and other variables in a forest canopy are provided by Wallace and Hobbs (Wallace and Hobbs, 2006). These structures are instantaneous moments in time when a certain variable (often potential temperature) has a sharp change in magnitude. These sharp departures are known to provide evidence for the overall depth of the BL. This information provides the knowledge and understanding necessary for trying to characterize different properties of the BL. It has also been shown that BL measuring instruments agree better during the winter months due to less convection and perturbations for the daily cycle (Sawyer and Li, 2013). This study looks at analyzing instrument correlation during non-winter months when the level of their accuracy is ultimately shown and their weaknesses are highlighted.

The fluxes of various gaseous constituents can provide helpful insight for observing BL progression and characteristics during the fall. In general, diurnal carbon dioxide fluxes are greater with warmer temperatures due to more photosynthesis, but ultimately depend on the capacity of the forest (Oke, 2002). This makes analyzing carbon dioxide more important to look at than when temperatures are below freezing. Carbon dioxide variations can also be helpful for what aerosols are associated with frontal passages as well as their overarching impact on BL depth. A previous study over northern Wisconsin looked at the passage of a low-pressure system and saw an increase in temperature, WVMR, wind speed, as well as a change in wind shear, all whilst carbon dioxide saw a rapid decrease (Hurwitz et al., 2004). The same experiment

concluded that frontal systems and squall lies can be associated with synoptic transport of carbon dioxide as well as the potential for deep vertical mixing between the free atmosphere and the surface. A study at the same location showed there was a significant decrease in carbon dioxide concentration followed by a slight increase before the front arrived and then a decreasing trend afterwards (Wang et al., 2007). It concluded that this was mostly correlated with horizontal advection as opposed to a different forcing. The study also showed high concentrations that were built up over the southern Great Plains due to a decrease in the rate of photosynthesis that was correlated with warm and dry air that was over Texas and Oklahoma. This information proves that it's important to look at a variety of spatial scales as well as different atmospheric and surface characteristics.

This investigation focused on when the University of Wisconsin – Madison's Space Science and Engineering Center (SSEC) had its Portable Atmospheric Research Center (SPARC) at the Ameriflux WLEF tall tower in Park Falls, Wisconsin. The SPARC is a trailer that was located at the tower site from September 13th-27th, 2016. The atmospheric data taken from this trailer in conjunction with the measurements from the WLEF tower are used to provide important insights for effectively analyzing diurnal BL development and evolution. How can the data from each instrument be used to show unique aspects of the BL? When compared with each other, what instruments provide clear uncertainty in its measurements? Furthermore, how do gaseous constituents and fluxes from the WLEF tall tower relate to lidar and interferometer-derived observations?

Methods

Site Characteristics

The Ameriflux WLEF television tall tower is located eight miles west of Park Falls, Wisconsin inside the Chequamegon-Nicolet National Forest (45.9°N, 90.3°W). Even though the tower is generally close to a city, there are no known significant sources of pollution in the nearby area. Surrounding the site is a 400-meter radius of deforested area with an area for parking directly next to the tower itself. There are also a couple small buildings near the base of the tower for television transmittance and instrumental housekeeping. The site consists of wetlands, upland forests, and is representative of typical upper-Midwestern forests (Desai et al., 2008, 2015). The region has a rough forest height of 20m and is characterized by 70% deciduous and 30% coniferous trees (Xu et al., 2017). The tower is 447m tall and continuously takes readings at 30m, 122m, and 396m. It measures a plethora of atmospheric variables such as carbon dioxide and methane concentrations, soil moisture, friction velocity, sensible heat, latent heat, wind speed, wind direction, WVMR, and temperature. During the time of data collection, the sensor used to measure latent heating, sensible heating, friction velocity, methane concentration, wind speed, and wind direction at 396m was down. In addition, the sensor measuring near-surface soil moisture was invalid as well. Nonetheless, the working sensors and wide variety of atmospheric characteristics measured were capable of measuring BL fluxes with great magnitude.

SPARC Trailer

The SSEC's SPARC is provided by the University of Wisconsin – Madison for data collection during this period. It is a ground-based trailer that is connected to a pickup truck and travels to a variety of locations throughout the year. It was created in 2014 and consisted of a revised version of the AERIbago, the SSEC's prior mobile lab that was in service for 20 years. This trailer was positioned on the ground right next to the tower and continuously collected data

over the entire two-week period. The SPARC trailer is outfitted with a host of elaborate instruments including a High Spectral Resolution Lidar (HSRL), Atmospheric Emitted Radiance Interferometer (AERI), Surface Meteorology Station (SurfaceMet), WindPro lidar, and a radiosonde receiving station.

HSRL

The ultimate function of the HSRL is to measure aerosols within the atmosphere, with an emphasis on lower altitudes. The lidar works by making calibrated measurements of backscatter from an emitted laser beam. Individual objects can be viewed by splitting the light being returned and comparing the backscatter and attenuation with each other. The HSRL has characteristics of a typical volume imaging lidar where it can present a three-dimensional structure of the atmosphere over time, create images of a large volume of the sky at one moment in time, and can create accurate averaged wind measurements. Typical lidars are often unreliable due to the size distributions of particles being highly variable. However, this lidar excels over traditional lidars by accurately observing the relationship between extinction and backscatter with regards to the size of the scattering particles, creating more reliable extinction cross sections.

The lidar measures two separate signals for aerosol and molecular scattering, which can be used to determine liquid and ice in the atmosphere. One channel gets the Doppler shift, which measures horizontal movements, while the other channel measures both the Doppler and aerosol characteristics. The difference between these two is used to obtain aerosol properties. A molecular scatter cross section can be created based on the Rayleigh scattering theory and an independently measured temperature profile. The HSRL then uses this molecular scattering as a calibration target for accurate atmospheric profiles. The lidar backscatter ratio is then created by comparing the aerosol lidar return to the molecular return and is used to combine both large and

small particles. Comparing the signals from the 532nanometer(nm) and 1064nm wavelengths is used to show the particle size since a 532nm-range particle looks small on the 1064nm projection. Prior studies using a Ramian lidar utilize these aerosol scattering ratios to determine mixed layer heights (Hicks et al., 2015). The aerosol backscatter cross section is of most importance for BL observances and is created via the lidar backscatter ratio and the molecular backscatter cross section. One general downfall is that observations during the afternoon are difficult to conclude due to the nature of the lidar. Wulfmeyer et al. suggest the need for lidars to have better transmitting powers and receiver efficiency for creating more accurate thermodynamic profiles (Wulfmeyer et al., 2015). Strong fluctuations of the HSRL projections are typical of evident rain showers. For typical ice and water clouds and most aerosols, the single scatter albedo at the 532nm wavelength is very close to unity. Linear depolarization is used to show the differences between ice and water clouds due to low linear depolarization and high backscattering being associated with circular particles. The linear depolarization ratio is the ratio between the perpendicular and parallel components of emitted light. In general, ice crystals and other irregularly shaped particles have a depolarization of 70%-50%. Water clouds have small optical depths giving low depolarizations and high amounts of scattering at larger optical depths, which increases the depolarization with the correlating penetration depth.

For this study, backscatter measured by the 532nm wavelength, 1064nm wavelength, 1064/532 aerosol backscatter ratio, and linear depolarization was used to measure BL properties based on the instrument's data. In addition, the HSRL data comes with a logbook explaining any possible errors in the equipment and housekeeping plots to make sure the hardware and software is functioning properly.

AERI

The AERI ultimately measures radiant energy that comes from the earth's atmosphere. It was initially created in the 1990's by the SSEC for the Department of Energy's Atmospheric Radiation Measurement Program. It utilizes a broad spectral content of 3-25μm and a larger spectral resolution of $0.5cm^{-1}$ for recognizing the difference between gaseous constituents and aerosols in the atmosphere. It has three main uses; creating temperature and water vapor vertical profiles, observing down welling infrared radiation from clouds and aerosols, and the measuring of ozone, carbon monoxide and methane. It has an accuracy of greater than 1.0% of a blackbody based on the surface ambient temperature. It does this through a continuous calibration based on a hot blackbody with a temperature set to 333K and an ambient blackbody that varies based on the nearby surrounding temperature. It creates spectral images of the atmosphere relying on sky views that are taken every 20 seconds.

The AERI utilizes a radiative transfer equation as well as starting temperature and water vapor characteristics from prior data to create retrievals more accurate than one wavenumber (Wayne F. Feltz et al., 1998). The instrument creates calibrated radiances from raw data by utilizing a front-end computer. The AERI has an auto-restart function, can operate in wide temperature ranges, a modular design that reduces the effects of contamination/dust, and real-time data that is adequately corrected (Knuteson et al., 2004). The interferometer is calibrated better than 1.0% of the ambient radiance, is capable of being created better than 0.2%, and is essentially a Fourier transform spectrometer but located on the ground (Knuteson et al., 2004). One downfall of the AERI instrument is that it lacks accurate data within and above cloud layers.

The instrument also needs to be combined with an algorithm for producing thermodynamic profiles of the atmosphere. The AERIprof algorithm was initially used by a statistical first-guess technique, but that often led to inadequate initial profiles and didn't show

the uncertainties in what was produced (Feltz et al., 2005). The new AERIoe algorithm has significant advancements such as being able to better reproduce atmospheric profiles for both cloudy and clear conditions in addition to being able to observe liquid cloud water properties (Turner et al., 2013). The algorithm has 85% of its temperature profiles and 70% of its water vapor profiles within the bottom 2km of the atmosphere. However, the algorithm still needs a priori information based on simulated AERI observations to create a clear solution and a relatively more stable inversion. When compared with radiosonde observations, the algorithm still produces some bias in temperature profiles during cloudy conditions. Nonetheless, the AERIoe algorithm is used during this data collection period for observing BL properties.

The AERI shows a base altitude of 470m which is used to correct the HSRL projections into being based on height above the instruments instead of on altitude. This altitude is further confirmed by radiosonde measurements showing a starting altitude of 473.9m. This conglomeration is used to effectively analyze the projected BL height and evolution over the course of the desired time periods. Vertical profiles of temperature, potential temperature, and WVMR from the AERI are used to emphasize BL development.

WindPro

The WindPro lidar is built by Halo Photonics and is a Stream Line Doppler Lidar System. It is used to create vertical profiles of wind speed and direction. The lidar measures the wind via frequency or changes in the wavelength of a given wave. The instrument also outputs a Signal-to-Noise Ratio (SNR) and a correlating standard deviation for creating effective analysis. A vector analysis of the wind can be fitted to a sine wave through the velocity-azimuthal display (VAD) (Browning and Wexler, 1968) approach (Pearson et al., 2009). This approach uses a beam being scanned in a cone at a specified altitude and averages the readings over hundreds of

meters and different time scales. If the flow is not laminar, a three-beam analysis may be created. While the data collected from this time isn't incredibly accurate, the higher SNR information can be used as a comparison with other instruments.

Radiosondes

The radiosondes during this time were sent next to the tower by those affiliated with the SPARC trailer. Radiosondes are paramount in the analysis of atmospheric conditions due to their often-high amount of accuracy and measurement. The information used by radiosondes for this period is the observed pressure, temperature and relative humidity. Over the two-week period, they were launched at various times and some errors were observed after the data started to be collected. This may have been from the radiosondes transmittance being affected by the television signal from the tower. Regardless, the radiosonde launched on September 24th saw little observable errors and can be used for consolidated analysis.

SurfaceMet

The SurfaceMet measures various atmospheric variables at the ground level. This instrument measures wind speed, wind direction, air temperature, and relative humidity. It also measures internal SPARC engineering values, temperature, relative humidity and electrical voltage for ensuring the trailer is functioning properly and taking in appropriate information. While not used tremendously, this data can be compared with the outputs from the HSRL, AERI and WindPro lidar for data correction at the surface.

Data Processing

Over the two-week period the SPARC trailer was at the site; the best analysis and comparison exists between September 23rd and 24th. This was concluded by observing the daily

reports from when faculty of the SSEC were at the site and was used to show any outlying errors across any of the instruments. Similarly, September 24th was the only day that a radiosonde had overlapping data with the WindPro lidar. The tower outputs information into a .csv file format which can be imported into MATLAB for creating plots. The HSRL and AERI create a network Common Data File that is then put through MATLAB functions to produce clear spatial projections. The WindPro lidar and radiosondes are also imported to MATLAB via .txt files to create single snapshots of the atmosphere at a specific time. All this information is compared together in the following sections for looking at BL depth and development.

Results

In order to effectively analyze the strengths and weaknesses of each measurement, the data from each instrument is compared with each other for each respective day. For simplicity of the expirement, appropriate figures are presented in terms of Coordinated Universal Time (UTC) along the x-axis and height above ground level in kilometers (km) along the y-axis. At the location of data collection, the timezone is U.S. Central Standard Time, which is UTC-6. Projected figures show 24 hour samples to accurately compare different BL characteristics that are displayed in Figure 1. The height of the projected results is presented from 0.0-2.0km above groundlevel. This range produces an accurate vertical profile for observing BL evolution over the selected periods. Single vertical snapshots were also computed to show the accuracy between each instrument side-by-side. In addition, the appendix shows more information that is correlated with the presented information for further BL analysis.

Stable Layer on September 23rd

The HSRL provides very accurate information and is capable to show show aerosol fluctuations in the BL better than any other instrument utilized in this experiment. The projected HSRL plots produce an image based on a matrix containing 68 by 2880 elements. The 68 elements are with respect to the height above the lidar while the 2880 correspond to the time variance. Figure 2 shows the 532nm backscatter and linear depolarization on September 23rd from 0:00-24:00UTC. The backscatter is measured in inverse meter steradians (1/(m sr)). While there is some noise at greater heights earlier in the collecition period, this provides insight for the characteristics of the BL shrinking due to a reduction in solar radiation. The sunset from the prior day occurred at 00:57UTC which is when a residual layer and correlating stable layer begins to form. On the contrary, the sun begins to rise at 12:51UTC. After the sunset from the prior day, the mixed layer shows to be overtaken by the newly-formed stable layer.

The height of the BL based on aerosol backscatter can be determined by looking for the sharpest gradient and observing the backscatter properties below that level. After 05:00UTC it becomes more clear there is a stable BL staying consistently between 0.2-0.3km. Above this layer there is an evident residual layer that can be further confirmed by the general neutrality reaching a peak height around 1.0km. On this same day, a decrease in potential temperature across all heights around 06:30UTC occurs when the HSRL shows the start of higher-level atmospheric mixing. While the 532nm and 1064nm backscatter (Figures A1 and A2) are often used for BL evolution, linear depolarization shows simlar results but provides newfound information with the shape of the aerosols. This becomes noteworthy when looking at gaseous atmopsheric components.

Carbon dioxide is one of the most commonly looked at greenhouse gases in today's society and can be crucial to look at for when certain layers evolve or disappear. Even though the

biggest changes of CO_2 happen daily based on photosynthesis rates, there are other factors that can cause concentrations (in parts per million) to fluctuate. Figure 4a shows the diurnal changing of CO_2 and the nonuniformity across three different heights over the night time when the stable layer was most present from the HSRL. To make these changes more applicable, Figure A4 provides a boxplot of CO_2 at 396m over the entire month of September. These changes in magnitudes can be compared with the diurnal departures to show the significance of each variability. Figure A5 also provides histograms of CO_2 at 396m for 1 hour, 3 hour, 10hour and 30 hour averages to show the true spread and frequency across the entire month. In addition to of CO_2 concentration, Figure 4 also shows sensible heat (b), latent heat (c), and friction velocity (d) at 30m and 122m over the same time. Sensible and latent heat is measured in watts per meter squarred (W/m^2) while friction velocity is measured in meters per second (m/s). Sensible heat is important to observe for BL development due to the surface sensible heat flux being proportional to the amount of turbulent kinetic energy that is created, which causes convection. Latent heat is related to BL characteristics through not being as thick when soils are moister and cooler from there being more net radiation being converted to latent heat. Friction velocity is also known as shear velocity and can be used to show characteristics of the flow near the surface. For appropriate analysis and consensus of observed trends, September 23rd is compared with September 24th to understand the relationship among these particular variables.

Mixed Layer on September 23rd

In addition to the somewhat clear stable layer, the HSRL and other instruments also show clear evidence for a mixed layer beginning to form just after sunrise. Its slowly increasing depth is also observed through the uniformity between the backscatter and linear depolarization. It is shown to increase linearly after sunrise and ends up reaching its peak height around 1.0km at

18:00UTC. Even though the BL depth reaches its greatest height during the first half of the day, its height varies by several hundred meters until sunset, which occurs just after the start of the September 24th collection period. The rise in depth is shown to be caused mostly by the increase in surface temperature, as shown in the AERI-generated plots.

Aerosol backscatter can be helpful to observe but taking a closer look at other variables over the same time and spatial plots can determine atmospheric processes during that period. Three important properties that are affected or influenced by atmospheric stability are temperature, potential temperature, and WVMR. For this experiment, the temperature is measured in degrees Celcius (°C), potential temperature in Kelvin (K), and the WVMR in terms of grams of water vapor per kilograms of dry air (g/kg). The vertical structure of potential temperature is of most significance due to being able to accruately describe where the atmosphere is stable, unstable, or neutral. The AERI projects these three variables (Figure 3) for the same spatiotemporal data that is projected by the HSRL (Figure 2). However, this data is presented with a grid size of 33 by 698 where 33 is the vertical component and 698 is the horizontal component. From the AERI plot, the sunrise and sunset can be further confirmed via the strong fluctuations in temperature near the surface. The BL development can also be shown through the positive slope in temperature. After 18:00UTC, the relatively stable and slightly decreasing BL depth is affiliated with a slight decrease in potential temperature until 24:00UTC. The WVMR can also be thought of having a great amount of fluctuation over the course of the day, but it still provides information that is helpful in analyzing BL characteristics. This is due to water vapor acting as the biggest and most variable greenhouse gas, which has a direct effect on the solar radiation balance near the surface.

The uniformity and presence of the convective BL is also evident by observing the uniformity of CO_2 across all three heights over this same time (Figure 4). The increase in BL depth and evolution is directly correlated with the increase in friction velocity at the exact same moment in time due from enhanced convection. Similarly, once the BL reaches its observed maximum, the friction velocity starts to decline rather rapidly showing a decrease in turbulent and convective motions. Between September 23rd and 24th, some similarities can be seen between the two while some differences clearly arise.

Stable and Residual Layers on September 24th

Even though the two analyzed periods occurred back-to-back, the HSRL shows some unique BL characteristics on the second day that differ from the first. The sunset occurred at 00:55UTC and the sun rose at 12:53UTC for the September 24th observation period (Figure 5). Just after the sun sets from September 23rd, the mixed layer begins to taper off and form a residual layer on top of the stable layer. More specifically, 00:00UTC-02:00UTC shows increasing boundary depth while 02:00-05:00UTC shows decreasing depth with a slightly higher backscatter. 06:00-08:00UTC shows a fair amount of mixing and unobservable boundary depth. The residual layer can be seen to fluctuate around 0.8km and the stable layer becomes more apparent starting at 08:00UTC. There are also interesting BL properties being evident starting at 10:00UTC. The distinction between the amount of backscatter between September 23rd and 24th show how the BL can vary significantly over such a short period. These results can be further confirmed when looking at AERI-derived plots.

Similar to its earlier counterpart, Figure 6 shows the same measurements as Figure 3 but for September 24th instead of September 23rd. Surface temperature variability based on the current BL state can be easier observed as shown from 00:00UTC and 02:00UTC where the

mixed layer begins to be taken over by the stable layer. This is consistent with HSRL showing the observed BL as shrinking. While potential temperature appears to have a somewhat homogenous profile, the small peaks at 02:00UTC, 07:00UTC, and 08:00UTC can be helpful for determining atmospheric stability at that moment in time. WVMR appears to still be more variable than the other measurements, however, observing its fluctuations in value at a fixed height can be helpful for further enhancing BL properties drawn from other variables or instruments. While water vapor is a crucial gas to look at, carbon dioxide is equally important and is strongly influenced by photosynthesis, respiration, anthropogenic forcings, wind, and other factors that make it pivotal to analyze for the future of our planet.

Measurements from the WLEF tower can be helpful in attempting to draw similar conclusions observed seen in the prior AERI data. Figure 7 presents the same information as Figure 4 but for a September 24th instead of September 23rd. There is still a clear separation between CO_2 across all three heights over the night when the stable layer is most evident, but the initial and ending time of disconnection is slightly different from the prior day. The 30m height also shows a detachment occuring earlier than when the 122m and 396m readings began to separate. There is a spike in CO_2 around 07:00UTC and then a local minimum occurring around 08:30UTC that appears to be relatively consistent with changes in potential temperature. Similarly, there is another spike in CO_2 around 12:00-13:00UTC that is related to the spike in potential temperature at the same time. However, concentrations generally begin to come together starting around 13:00UTC which is right when the sun began to rise.

Mixed Layer on September 24th

As shown before, the sunrise is paramount for the increase in surface temperature which creates more friction velocity and forces the mixed layer to develop in place of the stable and

residual layers. The HSRL shows this starting around 15:00UTC followed by an increase in BL depth until it reaches its relative maximum near 0.8km around 22:00UTC. The entrainment zone also begins to increase and is associated with a correlating increasing thickness in mixed layer. The growth of the mixed layer can similarly be shown from the AERI-derived temperature profile starting at 13:00UTC, just after sunrise. After this between 15:30-16:00UTC the concentrations of CO_2 appear to come together across all three heights but is more pronounced between the 396m and the other two shallower readings. This consolidation is consistent with a relative peak in temperature and slight decrease in potential tempearture. It is also associated with the BL depth increasing at a slow but steady rate. Sensible heat and latent heat show similar characteristics to September 23rd where there is a maximum reached somewhere between 17:00UTC and 19:00UTC. However, September 24th shows values that increase slightly leading up to reaching their maximum while September 23rd had rather consistent readings. Friction velocity shows similar traits to sensible heat and latent heat except the values on September 24th appear to increase leading up to the sunrise, while September 23rd showed slightly more variability.

Frontal Passage near 19:00UTC on September 24th

Collectively, all three plots from the AERI on September 24th (Figure 6) show an interesting characteristic starting at 19:00UTC where there is an evident sharp increase in temperature, potential temperature and WVMR at greater heights. The sharp changing in magnitudes occuring near 19:00UTC may be caused by a frontal system passing through the area. While some WLEF tower measurements in addition to the radiosonde and WindPro data don't provide any more helpful information for the interesting trend at 19:00UTC, the SurfaceMet can be worthy to look at. Figure 9 presents the surface pressure occurring on

September 24th and shows a slightly decreasing trend starting at 15:00UTC. It's concluded that there is only a 1.5hPa decrease in pressure during this observed frontal passage seen from the AERI measurements.

Radiosonde at 19:14UTC on September 24th

For this experiment, the radiosonde launched on September 24th had the most accurate readings of all of the radiosondes that were successfully sent over the entire two-week period. This is due to it having the most readily available data that wasn't obstructed by the towers transmittance. It also was the only radiosonde that had reasonable overlap with the WindPro. The ground crew that launched this radiosonde stated that the conditions were overcast with a slight break in the clouds at the time of launch. Figure 8 shows a comparison between the radiosonde and AERI for temperature as well as a comparison between the radiosonde and WindPro for wind speeds at 19:14UTC on September 24th. Due to radiosondes generally being much more accurate than lidars for height observations, this information is used for properly observing BL properties. However, the comparison between different instruments can help bring various inaccuracies to the forefront. The temperature plots have both the same vertical and horizontal axes. The wind plots have the same vertical axes but the horizontal axes vary, emphasizing the imprecision between the two instruments. The sharp contrasting radiosonde-derived temperature near 0.7km is characteristic of the height of the mixed layer at this moment in time. The continuing layer above this height is also related to the entrainment zone due to being statically stable. There also appears to be shifts in backscatter that are directly correlated with shifts in wind speed.

Discussion

Interpretation

The analyses performed from the information presented consists of observing an interrelation between different instruments, BL properties from a variety of measurements, as well as possible forcings and correlations amongst the data. The first is that the HSRL showed lacking evidence of a clear BL from 00:00UTC-05:00UTC. This may be a sign of fumigation where pollutants are brought down from the free atmosphere above and block the lidars signal of greater heights. While the capping inversion around this time isn't easy to recognize, the evolving mixed layer is clear in that it starts right after the sun rises.

The slowly increasing depth associated with the mixed layer is also observed due to the backscatter and linear depolarization uniformity reaching its peak height around 1.0km at 18:00UTC. The entrainment zone is also slightly capable of being observed just above the top of this uniformity. The temperature profile on this same day (Figure 3) doesn't provide a tremendous amount of BL characteristics but it does give evidence for solar radiation fluctuations. In particular, the increasing temperature starting just after sunrise shows the increase amount of incoming shortwave radiation being absorbed by the surface. There are also a few spikes in temperature and potential temperature that may be caused by AERI noise or atmospheric variability just after BL depth was shown to be increasing.

The uniformity and presence of the convective BL on this same day is also evident by observing the uniformity of CO_2 across all three heights over this same time (Figure 4). More specifically, between 13:00 and 14:00UTC there appears to be relatively high amounts of backscatter and low depolarization between the surface and 0.4km. While this may be one small coincidence, this is the exact moment when the concentrations start to become more homogeneous. In general, when the BL sees a relative maximum in height, there is a slight

correlation with sensible heat, latent heat and friction velocity also reaching their maximum values. It is shown that the BL can cool and have less convection with divergence of sensible heat. Latent heat is helpful to look at for similar reasons where a case study showed CO_2 uptake being positively correlated with latent heat flux and vegetation greenness (Bonan, 2008). One exception to this is the 122m reading for sensible heat and the 122m reading for latent heat. The causes for these departures are not well known.

For the AERI data on September 24th (Figure 6), there becomes some contrasting BL properties that are marginally different from what was observed on September 23rd. For example, the clear building of the BL exists between 14:00UTC-19:00UTC. For potential temperature, the isentropes from 00:00UTC-04:00UTC and 15:00UTC-20:00UTC change height consistently with the HSRL projections. However, the most prominent properties of this day compared to the previous day is the increase in temperature and WVMR, and decrease in potential temperature starting at 19:00UTC. The increase in temperature and WVMR are correlated with each other due to warmer air being able to hold more water and therefore becoming moister. Similar artifacts can be confirmed via the increasing equivalent potential temperature as shown in Figure A3. One striking observation across all three variables is that after 19:00UTC their magnitude appears to be relatively stable compared to the projections before this moment on the same day. To draw any conclusions, it's crucial to look at information presented from the WLEF tower.

While CO_2 doesn't show any significant implications with regards to the rapid changes seen at 19:00UTC by the AERI on September 24th, other WLEF measurements can confirm this AERI observance. Sensible and latent heats both see a sharp increase across both heights at this exact moment in time. While these maximums are generally related to temperature and WVMR values, they provide more evidence that this observation isn't an instrumental failure. Friction

velocity also shows a relative maximum occuring near the same moment but not as pronounced as seen from the sensible and latent heat values.

Uncertainty

While some conclusions can be made and confirmed by collective analysis between the instruments used, there is still a great deal of uncertainty in the conclusions drawn. Due to the variability across all of the instruments, it becomes difficult to accurately deduce the BL height at any moment in time for both collection periods. This makes it more appropriate to look at BL characteristics as opposed to the depth and its concomitant evolution. For example, it's difficult to derive the height for 00:00UTC-05:00UTC on September 23rd (Figure 2) due to an external factor preventing the HSRL from measuring heights greater than 0.5km. One caveat is that there lacks significant evidence of a surface layer strictly based on the aerosol backscatter and linear depolarization. The sharp decreases in temperature and potential temperature on this same day at 04:00UTC and 16:00UTC don't have any significant causations that can be concluded from other data. The AERI also gives more uncertainty in upper-level observations from 12:00UTC-19:00UTC on September 24th when attempting to acknowledge the capping inversion or entrainment zone. Some difficulties also arise when attempting to find a clear entrainment zone, especially after 22:00UTC.

When comparing the radiosonde results to the AERI-derived vertical temperature profile, it's clear that there is quite some discrepancy. The AERI shows roughly the same values and trends at lower heights but that accuracy begins to taper off rather quickly with an increasing height. While this shows that the temperature profiles derived from the AERI may not be the most accurate, the BL characteristics of the atmosphere that are observed by the AERI are still confirmed by the WLEF tower's measurements. Comparing the radiosonde's wind speed with

what was observed from the WindPro at the same moment in time shows additional inconsistency. One downfall evident from the WindPro is the difference in wind speed magnitudes when compared with the radiosonde. While the WindPro very roughly shows similar inversion layers, the overall inaccuracy in its measurement make it an invalid tool for observing BL characteristics for this two-day comparison.

While initial thoughts suggested there might be a frontal passage going through the site at 19:00UTC, the SurfaceMet shows only a slight decrease in pressure that is only a couple hectopascal's (hPa) in strength over 8 hours. It is difficult to conclude why this drop in pressure isn't paramount, as would be expected by the AERI. More observations and analysis at this moment in time from other instruments would prove to be beneficial. To further confirm there wasn't a strong frontal passage going through, previous synoptic and mesoscale weather maps were closely analyzed. Prior radar that was analyzed on mesonet.agron.iastate.edu and mesoscale maps on wpc.ncep.noaa.gov didn't show any significant passages over this time. Additionally, they showed almost no rainfall at all for any location surrounding the site. These historic maps don't provide a tremendous amount of accuracy in producing significant conclusions showing that there is still a possibility of a front going through at this moment. After looking at numerous resources, it becomes difficult to provide certainty for a front passing through that matches the characteristics seen from both the AERI and SurfaceMet.

Implications/future work

Further analysis and statistical significance is required to show any true BL characteristics and its concomitant associations. It is crucial to have a time when there was more than one radiosonde being launched that had successful readings. It's also paramount to have multiple instruments taking clear readings without any gaps in data. This is further confirmed by

the WindPro needing the SNR range to be >.002 in hopes of seeing any type of data. In hopes of utilizing the WindPro data, the SNR range would need to be much higher than .002, perhaps .008 and above.

Conclusion

The consensus of this experiment confirms that a variety of instruments need to be utilized to draw any conclusions of various atmospheric phenomena. This study analyzed BL properties through a HSRL, AERI, WindPro lidar, radiosonde, SurfaceMet, and the WLEF Tall Tower. It is confirmed that ground-based instruments provide some insight for how BL evolves diurnally but specifics are lacking. While there was some uncertainty observed throughout the experiment, interesting interpretations can be shown throughout each instrument.

The HSRL appeared to be relatively accurate in deducing BL characteristics that are often typical as provided by scientific literature. The depths of the mixed layer, residual layer, and stable BL are easiest to be seen through their relative uniformity in aerosol backscatter and linear depolarization. The capping inversion, entrainment zone and free atmosphere are difficult to deduce based strictly on backscatter. This is due to the characteristic behavior of lidars where signals are often obstructed from lower aerosols or reflected in directions that are not capable of being received by the instrument.

The AERI provided relatively consistent vertical profiles of temperature, potential temperature and WVMR over the same periods observed by the HSRL. These profiles can provide information that is related to the amount of incoming solar radiation, which is directly related to the thickness and progression of the BL. Decreases in potential temperature can sometimes be seen to be related to atmospheric mixing at higher elevations due to more

convection being evident. September 24th showed potential temperature varying directly with the HSRL-derived BL depths and is confirmed by the relation of potential temperature to atmospheric stability.

The information provided from the WLEF tall tower wasn't characteristic of helping conclude BL depths, but it rather helped give strength in the BL conclusions drawn from other instruments. For both days, CO_2 concentrations showed clear separation across each height during the night time. Immediately after the sun rose, the concentrations across all three heights became more uniform, which is characteristic of a typical BL mixed layer. The amount of convection for each day was also further confirmed by the friction velocity even though the measurements were only provided up to 122m above the surface. Due to this caricature, the friction velocity also appeared to be directly correlated with the BL depth across various instances in time. The sensible and latent heat fluxes were helped show more explaination as to what was seen by AERI data. While these fluxes are related to temperature and WVMR, they provide more strength into the accuracy in each instrument.

September 24th showed an interesting trend in the latter half of the collection period that was strikingly different than what was seen over September 23rd. There was an evident sharp increase in temperature, increase in WVMR, and decrease in potential temperature around 19:00UTC. This sharp contrast is confirmed by analysis of the sensible and latent heating at this moment in time. Looking at the surface pressure from the SurfaceMet showed there being a slight decrease in pressure over this time, but the magnitude of the changes was not significant enough to produce what was seen in other instruments. Prior weather maps were also looked at but no strong conclusions can be drawn to deduce the reasoning for this occurrence.

The one radiosonde launched during these two days was sent on September 24th and was directly compared with vertical snapshots of AERI-derived temperature and WindPro-derived wind speeds. This direct analysis showed a tremendous amount of inaccuracy in the AERI and WindPro measurements for this specific moment. This could be due to significant noise at this specific reading or perhaps due to the uncertainties drawn naturally from each instrument. This experiment doesn't provide any possible causations for these discrepancies other than that they clearly occur.

This analysis states that there needs to be more atmosphere-based measurements and calculations that need to be compared to ground-based instruments for effective analysis and consensus among BL characteristics. More studies need to be conducted to confirm the correlations seen throughout this experiment. It would be beneficial for the WLEF tower to have a working soil moisture probe as well as a working 396m sensor for sensible heat, latent heat and friction velocity. It would also be helpful if the WindPro provided more values above a higher SNR threshold. The SPARC travels frequently to different parts of the nation and an intercomparison between this data and other locations can provide new insights for what is concluded from this experiment.

Acknowledgements

Ankur Desai for support and the SSEC for funding the experiment with an emphasis on assistance from Tim Wagner, Wayne Feltz, Erik Olson, and Edwin Eloranta.

Figures

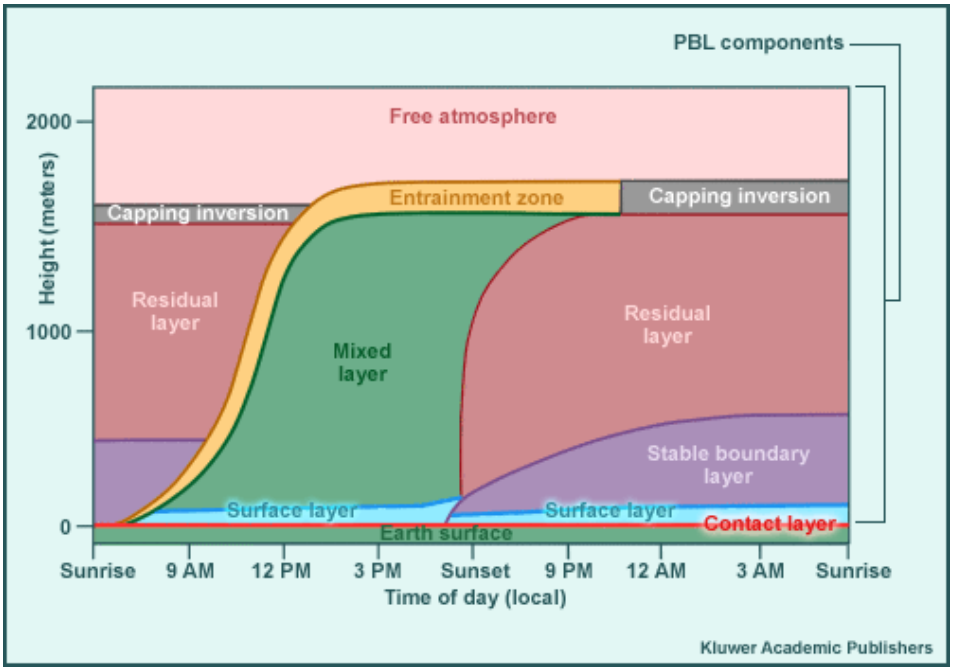

Figure 1. Typical boundary layer evolution over the course of 24 hours emphasizing the differences between nocturnal and daily characteristics. While there are a tremendous number of layers, it's difficult to observe the capping inversion and entrainment zone from most instruments in this experiment being ground-based. Image provided by meted.ucar.edu.

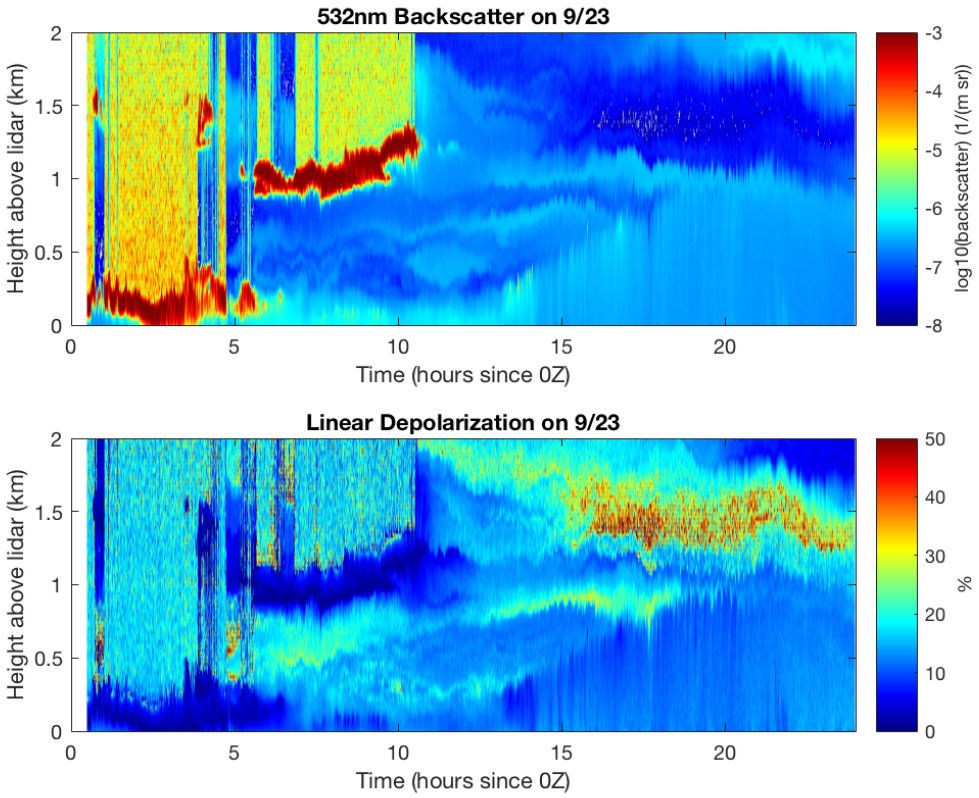

Figure 2. Aerosol 532nm backscatter (top) and linear depolarization (bottom) from 00:00UTC-24:00UTC on September 23rd derived from the HSRL. There exists a clear distinction between the BL uncertainty before 13:00UTC and the evident mixed layer afterwards.

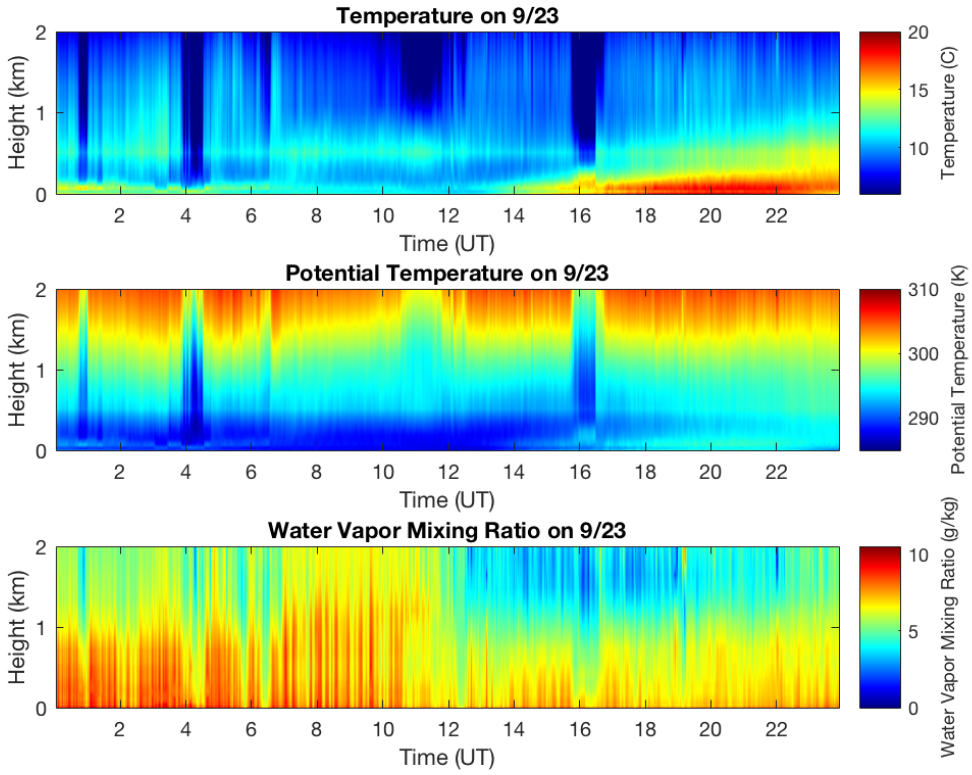

Figure 3. Temperature (top), potential temperature (middle) and WVMR (bottom) from 00:00UTC-24:00UTC on September 23rd derived from the AERI. All three variables provide windows (01:00UTC, 04:00UTC and 16:00UTC) when there may be errors with the instrument.

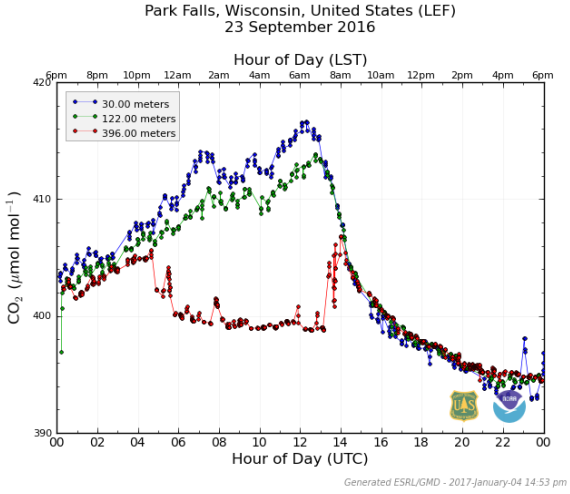

a.

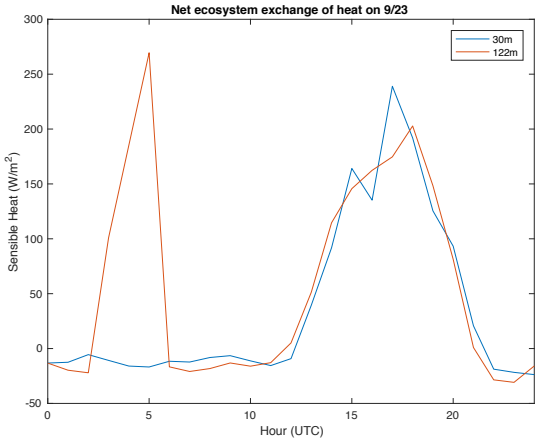

b.

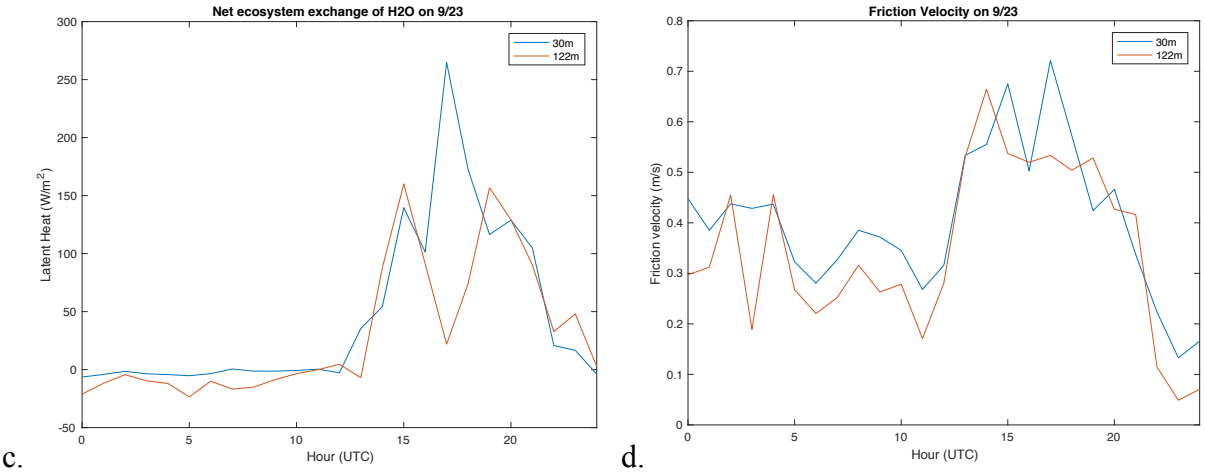

c. d.

Figure 4. WLEF tower measurements of a) carbon dioxide, b) sensible heat, c) latent heat, and d) friction velocity for 00:00-24:00UTC on September 23rd. The sensible and latent heat fluxes appear to have quite some variability between the two heights measured.

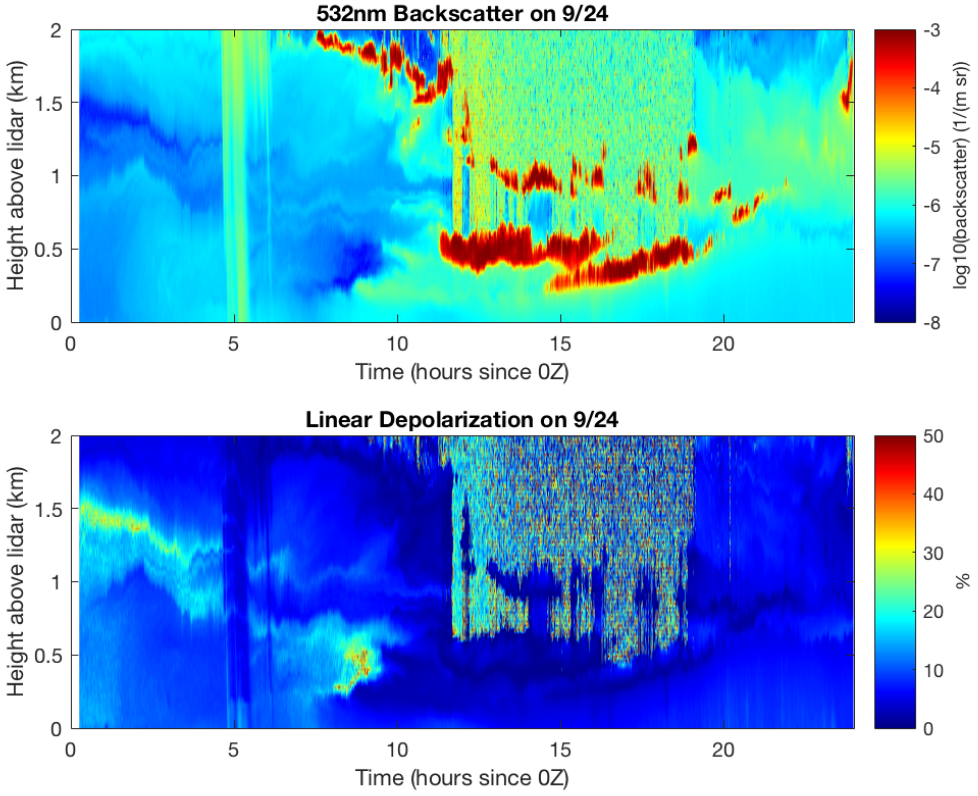

Figure 5. Aerosol 532nm backscatter (top) and linear depolarization (bottom) from 00:00UTC-24:00UTC on September 24th derived from the HSRL. Contrasting Figure 2, the first half of the

data collection shows the leftover mixed layer while the second half is slightly harder to deduce from the high backscatter at lower heights.

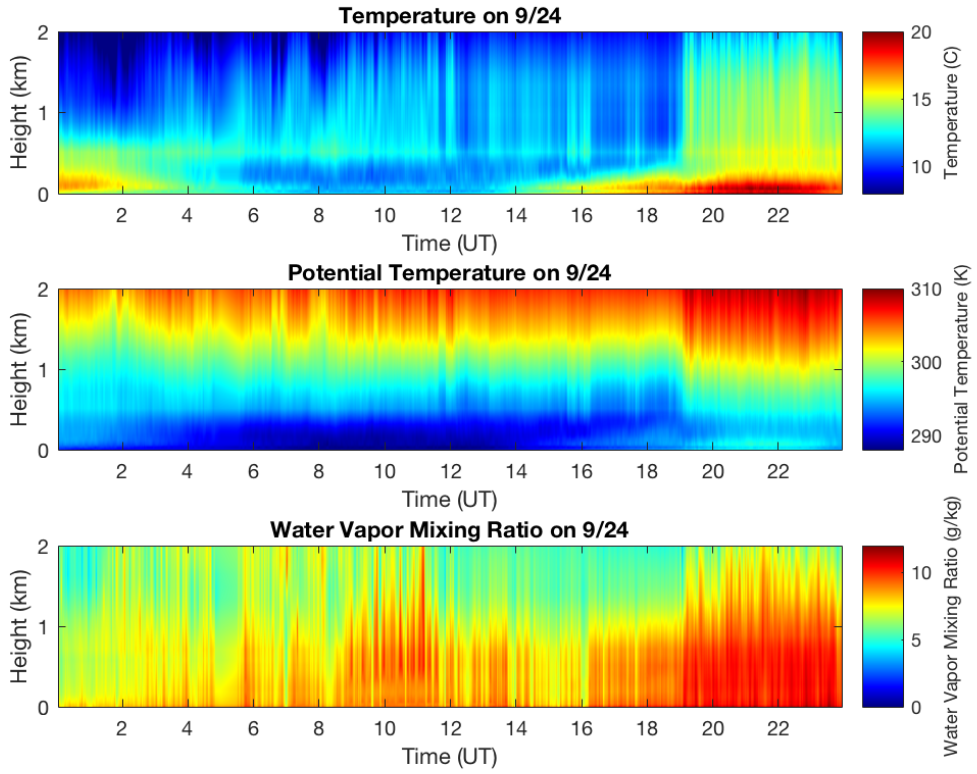

Figure 6. Temperature (top), potential temperature (middle) and WVMR (bottom) from 00:00UTC-24:00UTC on September 24th derived from the AERI. Note the instantaneous spike in temperature and WVMR and corresponding decrease in potential temperature at 19:00UTC.

a.

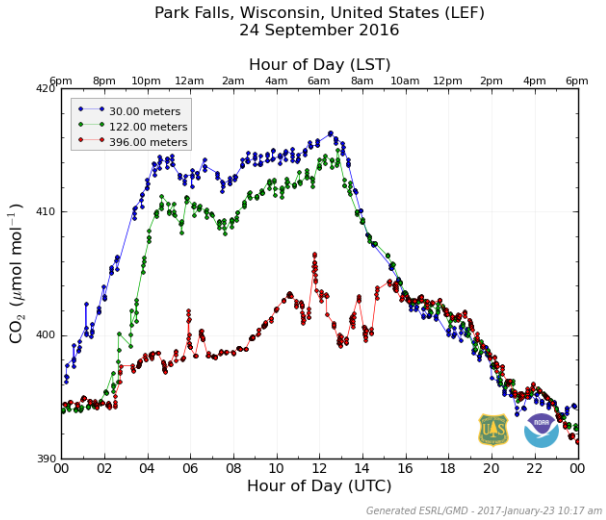

b.

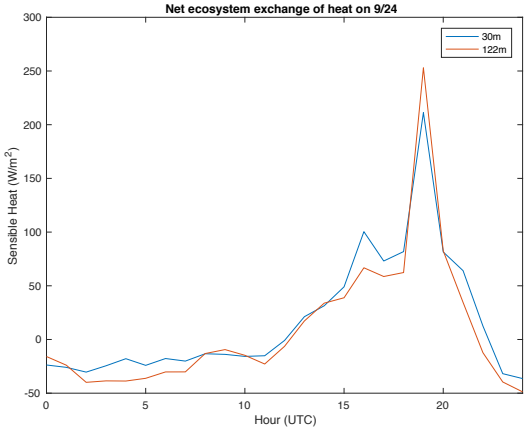

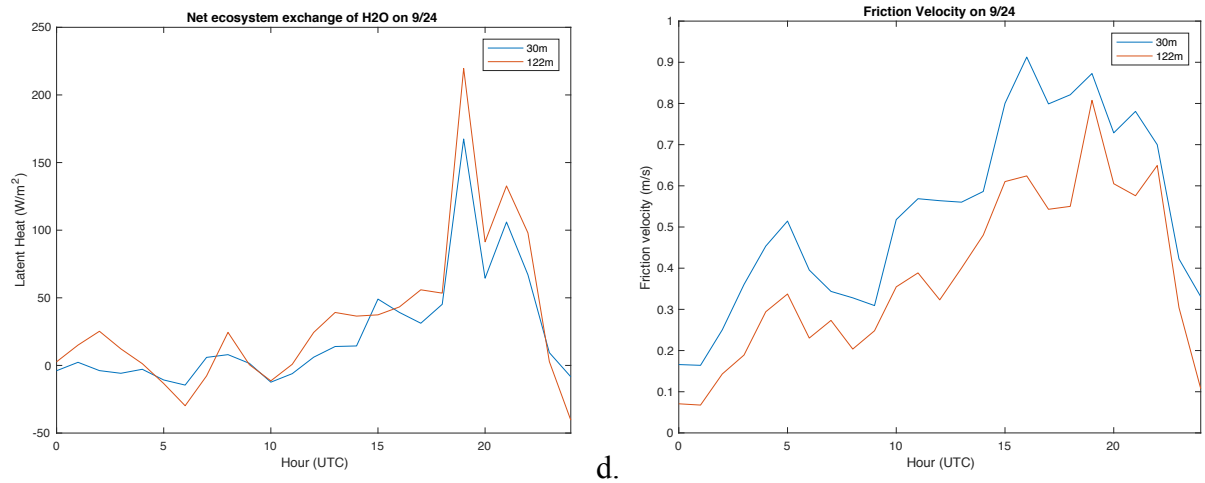

c. d.

Figure 7. WLEF tower measurements of a) carbon dioxide, b) sensible heat, c) latent heat, and d) friction velocity for 00:00-24:00UTC on September 24th. The relative magnitudes in sensible heat, latent heat, and friction velocity appear to occur when the AERI shows sharp departures from normal.

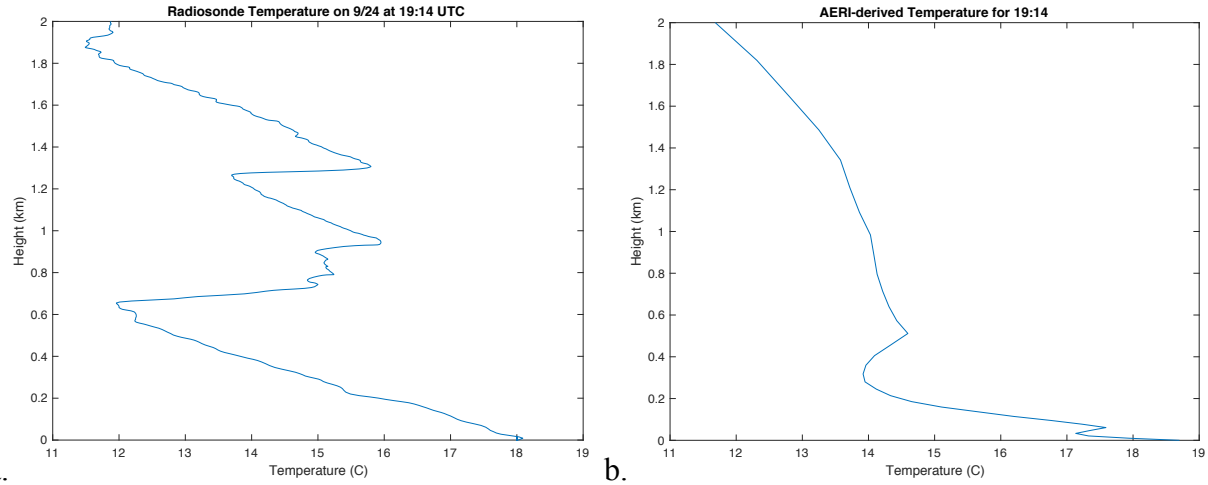

a. b.

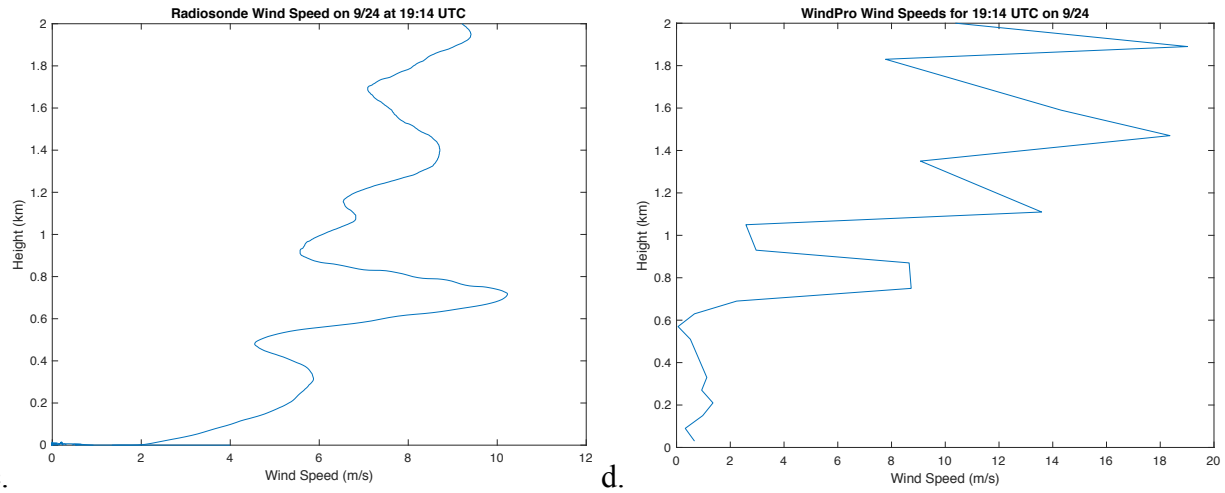

c. d.

Figure 8. A single vertical snapshot of the atmosphere at 19:14UTC on September 24th for a) radiosonde-derived temperature, b) AERI-derived temperature, c) radiosonde-derived wind speed, and d) WindPro-derived wind speed when SNR>.002. Some differences between each plot may exist due to lack of data available at this moment in time.

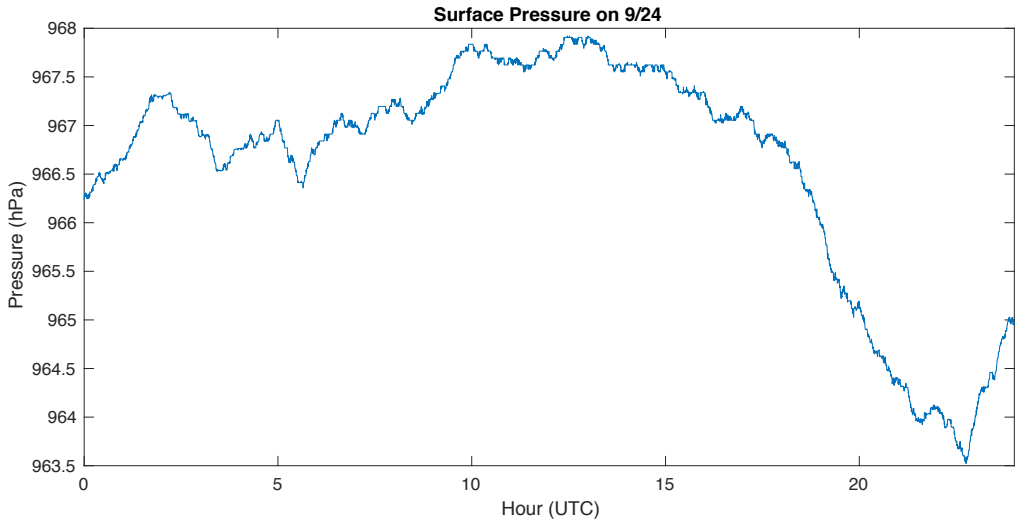

Figure 9. Surface pressure on September 24th derived from the SurfaceMet. While there is a clear drop in pressure starting around 14:00UTC, the magnitude of the changes don't provide significant evidence for a strong frontal passage.

APPENDIX

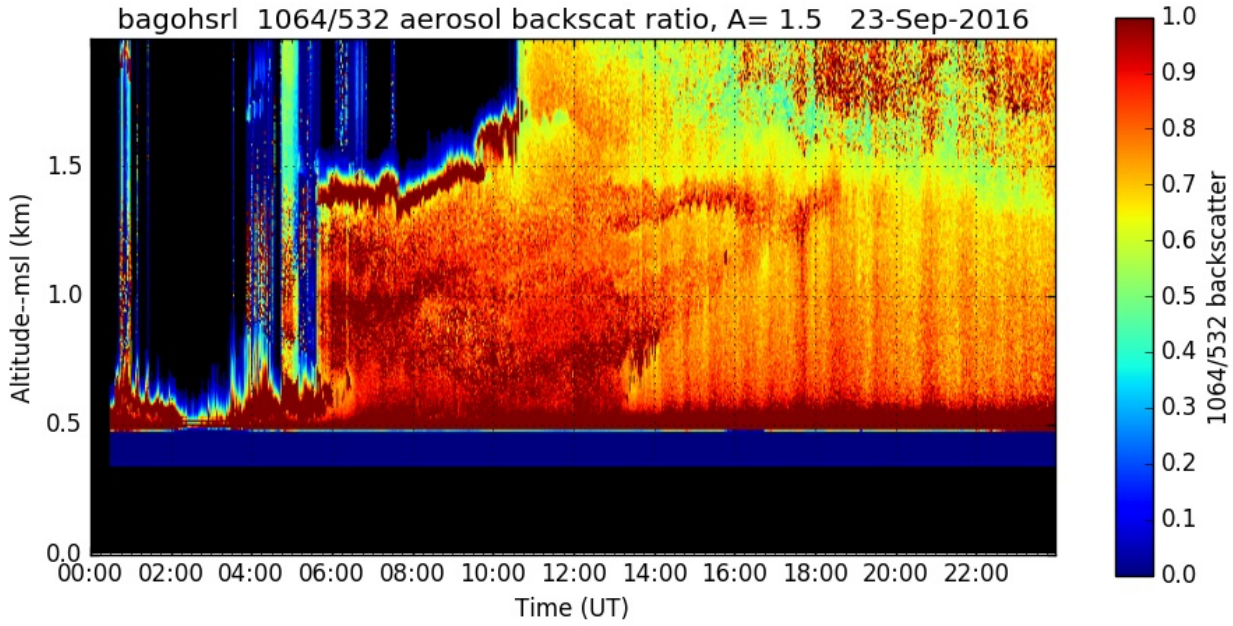

Figure A1. 1064/532nm backscatter ratio on September 23rd produced via hsrl.ssec.wisc.edu. This projection helps show greater variability in BL characteristics than 532nm and linear depolarization alone.

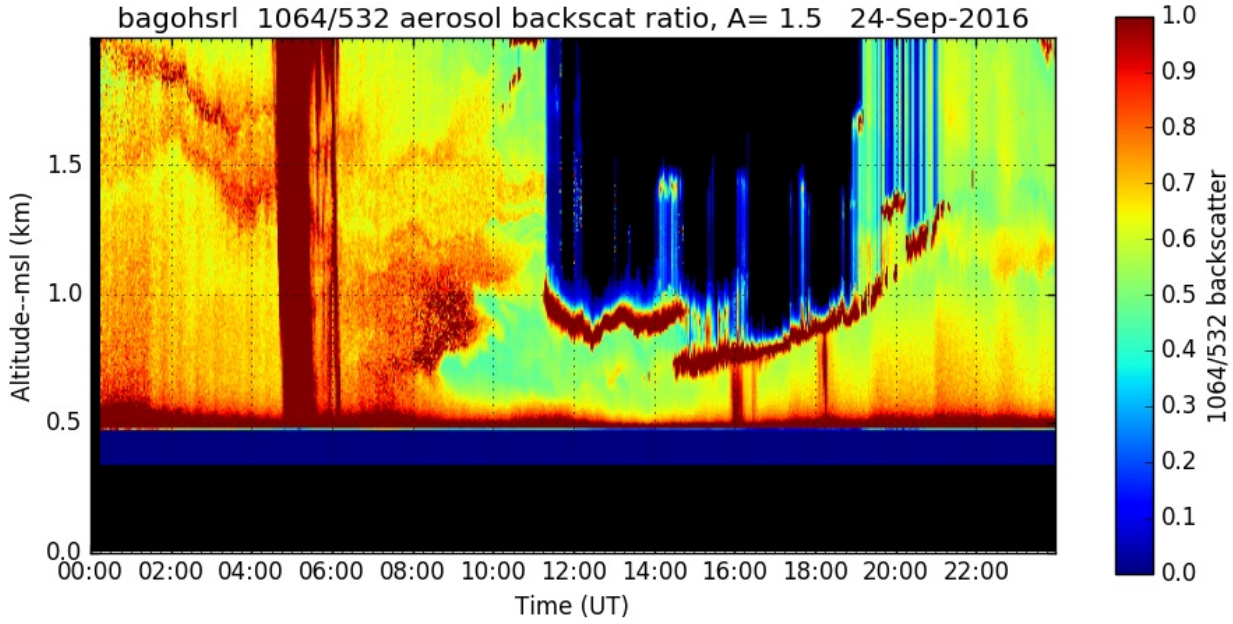

Figure A2. 1064/532nm backscatter ratio on September 24th produced via hsrl.ssec.wisc.edu. Compared with Figure 5, it's easier to observe more BL characteristics below the relative maximums in backscatter.

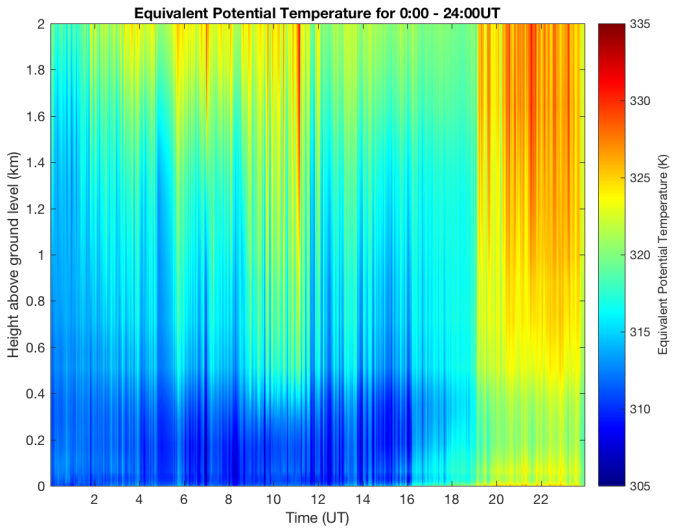

Figure A3. Equivalent potential temperature on September 24th for 00:00UTC-24:00UTC showing a sharp instantaneous increase starting at 19:00UTC. Like Figure 6, there is a strong increase occurring near 19:00UTC.

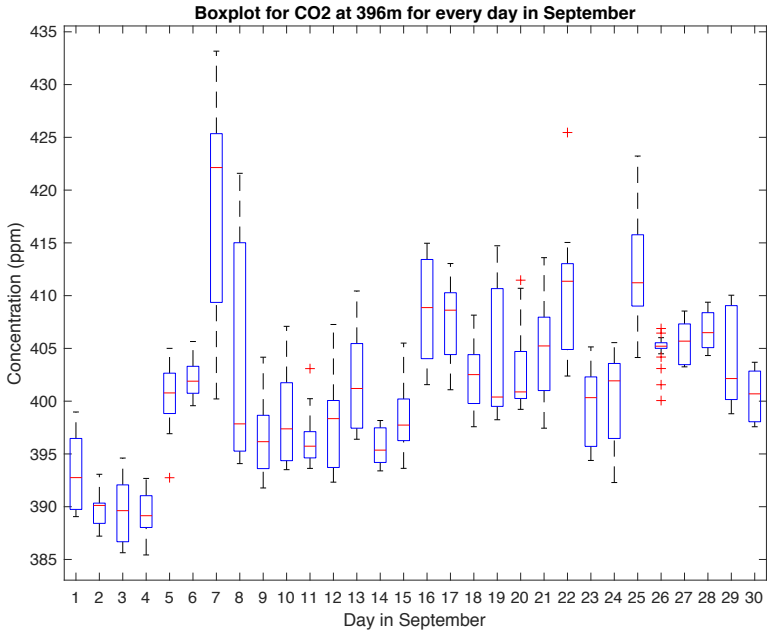

Figure A4. Boxplot for CO_2 at 396m over the entire month of September 2016. This figure provides insight for how the concentrations on September 23rd and 24th fluctuate compared with other days throughout the month. The red line represents the median value on that day and the blue box represents values within the first and third quantiles. The black line extending from the box shows the minimum and maximum values observed.

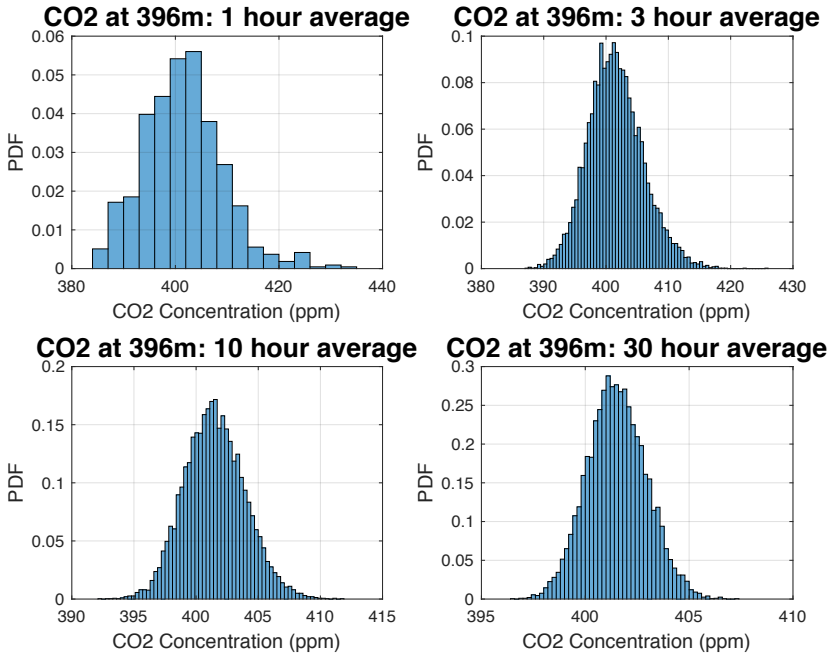

Figure A5. Histograms of CO_2 concentrations at 396m over the entire month of September based on 1 hour, 3 hour, 10 hour, and 30 hour averages. The concentrations are shown in relation to probability density functions (PDF). The spread of these concentrations can be compared with the differences seen on September 23rd and 24th for analyzing their significance.

References

Betts, A. K., and Ball, J. H. (1995): The FIFE surface diurnal cycle climate. *Journal of Geophysical Research*, **100**, D12, 25679–25693, doi:10.1029/94JD03121.

Betts, A. K., and Ball, J. H. (1998): FIFE Surface Climate and Site-Average Dataset 1987–89.

Journal of the Atmospheric Sciences, **55**, 7, 1091–1108, doi:10.1175/1520-0469(1998)055<1091:FSCASA>2.0.CO;2.

Bonan, G. B. (2008): *Ecological Climatology: Concepts and Applications* (2nd ed.). Cambridge: Cambridge University Press, doi:10.1017/CBO9781107339200.

Browning, K. A., and Wexler, R. (1968): The determination of kinematic properties of a wind field using Doppler radar. *Journal of Applied Meteorology and Climatology*, **7**, 1, 105–113, doi:10.1175/1520-0450(1968)007<0105:TDOKPO>2.0.CO;2.

Desai, A. R., Davis, K. J., Senff, C. J., Ismail, S., Browell, E. V., Stauffer, D. R., and Reen, B. P. (2006): A Case Study on the Effects of Heterogeneous Soil Moisture on Mesoscale Boundary-Layer Structure in the Southern Great Plains, U.S.A. Part I: Simple Prognostic Model. *Boundary-Layer Meteorology*, **119**, 195–238, doi:10.1007/s10546-005-9024-6.

Desai, A. R., Noormets, A., Bolstad, P. V, Chen, J., Cook, B. D., Davis, K. J., … Wang, W. (2008): Influence of vegetation and seasonal forcing on carbon dioxide fluxes across the Upper Midwest , USA : Implications for regional scaling, **148**, 288–308, doi:10.1016/j.agrformet.2007.08.001.

Desai, A. R., Xu, K., Tian, H., Weishampel, P., Thom, J., Baumann, D., … Kolka, R. (2015): Agricultural and Forest Meteorology Landscape-level terrestrial methane flux observed from a very tall tower. **201**, 61–75, doi:10.1016/j.agrformet.2014.10.017.

Feltz, W. F., Howell, H. B., Knuteson, R. O., Woolf, H. M., Turner, D. D., Mahon, R., … Smith, W. L. (2005): Retrieving Temperature and Moisture Profiles from AERI Radiance Observations : AERIPROF Value-Added Product Technical Description. DOE/SC-ARM/TR-066, 41 pp. [Available online at http://www.arm.gov/publications/tech_reports/arm-tr-066.pdf.]

Feltz, W. F., Smith, W. L., Knuteson, R. O., Revercomb, H. E., Woolf, H. M., and Howell, H. Ben. (1998): Meteorological Applications of Temperature and Water Vapor Retrievals from the Ground-Based Atmospheric Emitted Radiance Interferometer (AERI). *Journal of Applied Meteorology*, **37**, 857–875, doi:10.1175/1520-0450(1998)037<0857:MAOTAW>2.0.CO;2.

Hicks, M., Sakai, R., and Joseph, E. (2015): The Evaluation of a New Method to Detect Mixing Layer Heights Using Lidar Observations. *American Meteorological Society*, 2041–2051, doi:10.1175/JTECH-D-14-00103.1.

Hurwitz, M. D., Ricciuto, D. M., Bakwin, P. S., Davis, K. J., Wang, W., Yi, C., and Butler, M. P. (2004): Transport of Carbon Dioxide in the Presence of Storm Systems over a Northern Wisconsin Forest. *Journal of the Atmospheric Sciences*, **61**, 5, 607–618, doi:10.1175/1520-0469(2004)061<0607:TOCDIT>2.0.CO;2.

Knuteson, R. O., Revercomb, H. E., Best, F. A., Ciganovich, N. C., Dedecker, R. G., Dirkx, T. P., … Tobin, D. C. (2004): Atmospheric Emitted Radiance Interferometer. Part II: Instrument performance. *Journal of Atmospheric and Oceanic Technology*, **21**, 12, 1777–1789, doi:10.1175/JTECH-1663.1.

Oke, T. R. (2002): *Boundary Layer Climates* (2nd ed.). Routledge: Taylor & Francis Group.

Pearson, G., Davies, F., and Collier, C. (2009): An Analysis of the Performance of the UFAM Pulsed Doppler Lidar for Observing the Boundary Layer. *Journal of Atmospheric and Oceanic Technology*, **26**, 2, 240–250, doi:10.1175/2008JTECHA1128.1.

Sawyer, V., and Li, Z. (2013): Detection, variations and intercomparison of the planetary boundary layer depth from radiosonde, lidar and infrared spectrometer. *Atmospheric Environment*, **79**, 518–528, doi:10.1016/j.atmosenv.2013.07.019.

Turner, D. D., and Lohnert, U. (2013): Information Content and Uncertainties in Thermodynamic Profiles and Liquid Cloud Properties Retrieved from the Ground-Based Atmospheric Emitted Radiance Interferometer (AERI). *Journal of Applied Meteorology and Climatology*, **53**, 752–771, doi:10.1175/JAMC-D-13-0126.1.

Wallace, J. M., and Hobbs, P. V. (2006): *Atmospheric Science: An Introductory Survey* (2nd ed.). Amsterdam: Elsevier Academic Press.

Wang, J.-W., Denning, A. S., Lu, L., Baker, I. T., Corbin, K. D., and Davis, K. J. (2007): Observations and simulations of synoptic, regional, and local variations in atmospheric CO2. *Geophysical Research*, **112**, doi:10.1029/2006JD007410.

Wulfmeyer, V., Hardesty, R. M., Turner, D. D., Behrendt, A., Cadeddu, M. P., Girolamo, P. Di, … Zus, F. (2015): A review of the remote sensing of lower tropospheric thermodynamic profiles and its indispensable role for the understanding and the simulation of water and energy cycles. *American Geophysical Union*, 53, 819–895, doi:10.1002/2014RG000476.

Xu, K., Metzger, S., and Desai, A. R. (2017): Upscaling tower-observed turbulent exchange at fine spatio-temporal resolution using environmental response functions, **232**, 10–22, doi:10.1016/j.agrformet.2016.07.019.